Precise Determination of Blackbody Radiation Shifts in a Strontium Molecular Lattice Clock

B. Iritani[1, *], E. Tiberi[1, *], W. Skomorowski[2], R. Moszynski[3], M. Borkowski[1, 4, 5] and T. Zelevinsky[1, †]

[1]*Department of Physics, Columbia University, 538 West 120th Street, New York, NY 10027-5255, USA*
[2]*Centre of New Technologies, University of Warsaw, Banacha 2c, 02-097 Warsaw, Poland*
[3]*Quantum Chemistry Laboratory, Department of Chemistry,*
University of Warsaw, Pasteura 1, 02-093 Warsaw, Poland
[4]*Van der Waals-Zeeman Institute, Institute of Physics, University of Amsterdam,*
Science Park 904, 1098 XH Amsterdam, The Netherlands
[5]*Institute of Physics, Faculty of Physics, Astronomy and Informatics,*
Nicolaus Copernicus University, Grudziadzka 5, 87-100 Torun, Poland
(Dated: June 6, 2023)

Molecular lattice clocks enable the search for new physics, such as fifth forces or temporal variations of fundamental constants, in a manner complementary to atomic clocks. Blackbody radiation (BBR) is a major contributor to the systematic error budget of conventional atomic clocks and is notoriously difficult to characterize and control. Here, we combine infrared Stark-shift spectroscopy in a molecular lattice clock and modern quantum chemistry methods to characterize the polarizabilities of the Sr_2 molecule from dc to infrared. Using this description, we determine the static and dynamic blackbody radiation shifts for all possible vibrational clock transitions to the 10^{-16} level. This constitutes an important step towards mHz-level molecular spectroscopy in Sr_2, and provides a framework for evaluating BBR shifts in other homonuclear molecules.

Frequency standards are the cornerstone of precision measurement. Among them, optical atomic clocks set records in both precision and accuracy, and are poised to redefine the second [1–7]. As a complement to these atomic systems there is a growing interest in precision measurements with molecules [8–12]. The simple structure of homonuclear diatoms, such as Sr_2, makes these molecules ideal testbeds to probe new avenues for fundamental physics research, including searches for corrections to gravity at short distances [13–16] and tests of the temporal variation of fundamental constants [12, 17–26]. As such, there is interest in improving techniques for molecular spectroscopy. Even for ultra-precise atomic clocks, the blackbody radiation (BBR) shift remains a primary contribution to the overall uncertainty of the clock measurement [3, 4, 27–32], and is notoriously difficult to control and characterize [33–35]. State-of-the-art evaluations of BBR shift rely on precise measurements of the differential dc polarizability of the clock states in conjunction with robust modeling of dynamic contributions [36–40].

In our previous work, we demonstrated record precision for a molecular lattice clock by measuring a 32 THz transition between two vibrational levels in ultracold Sr_2 molecules, reaching a 4.6×10^{-14} systematic uncertainty [41]. Estimates of the BBR contribution to this uncertainty relied on preliminary theoretical modelling of polarizabilities that lacked experimental verification. In this Letter, we determine room-temperature BBR shifts for our molecular clock to the 10^{-16} level. To do so, we employ modern quantum chemistry methods to determine the differential polarizabilities for all vibrational clock transitions. We then verify our theory directly by measuring ac Stark shifts induced by a 1.95 µm laser for a wide variety of molecular clock transitions (Fig. 1). Given this combined experimental and theoretical picture, we develop a complete description of the BBR effect. Below, we describe a robust theoretical model, experimentally validate and extend

this model to other relevant wavelengths, and determine the BBR shift for all vibrational states of our Sr_2 molecules.

The experimental sequence closely follows that of our previous works [9, 41–43]. Briefly, a $2\,\mu$K sample of ultracold strontium atoms is trapped in a one-dimensional horizontal optical lattice in the near-infrared. We form weakly bound molecules by applying a photoassociation pulse tuned to the $-353\,$MHz 1_u resonance [44]. This bound state predominantly decays to a pair of rotational $J = 0, 2$ states of the least bound vibrational state, $v' = 62$, in the ground state potential. For a given measurement, we apply a two-photon Raman pulse to probe the selected clock transition, and detect the number of remaining $v' = 62$ molecules by photodissociating them near the $^1S_0+^3P_1$ threshold [45] and counting the recovered atoms. Unless otherwise specified, we always refer to rotationless $J = 0$ states in the electronic ground state potential, and list the lower energy state first for a given transition, regardless of where the molecular population is initialized.

Our clock spectroscopy relies on narrow-linewidth Raman transitions between the least bound $v' = 62$ vibrational state and a selection of more deeply bound vibrational states v of the Sr_2 molecule [shown for $0 \leftrightarrow 62$ in Fig. 1(a)]. We address each of these transitions via intermediate states v'' in the electronically excited $(1)\,0_u^+$ potential. The vibrational splittings are determined by the difference in the pump ($v' \rightarrow v''$) and anti-Stokes ($v'' \rightarrow v$) laser frequencies. We select intermediate states with favorable Franck-Condon factors for the pump and anti-Stokes transitions for each interrogated pair of clock states (Table I). In order to address clock states throughout the potential well, we use 3 different intermediate states in the excited $(1)\,0_u^+$ potential: $v'' = 11$ [at $-57\,084\,156.51(12)$ MHz from the $^1S_0+^3P_1$ threshold], $v'' = 15$ [at $-48\,855\,512.13(18)$ MHz], and $v'' = 16$ [at $-47\,036\,433.95(23)$ MHz]. The selection of intermediate states is a balancing act between available lasers and transition
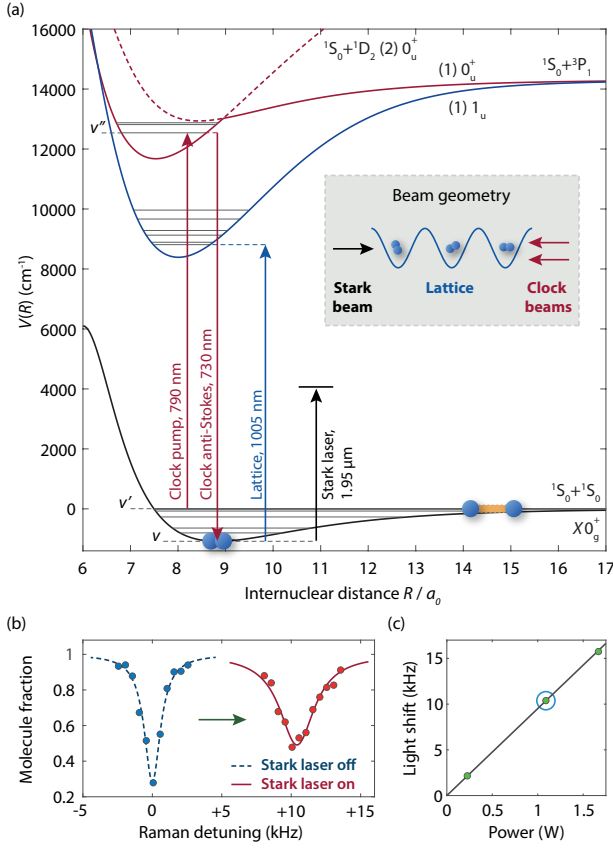
FIG. 1. Stark shift spectroscopy in a Sr_2 molecular clock on the example $0 \leftrightarrow 62$ transition. (a) Our molecular clock relies on narrow two-photon Raman transition via an intermediate state in the $(1)\, 0_u^+$ (red arrows) in a magic lattice that couples the deeply-bound clock state v to an excited $(1)\, 1_u$ state (blue arrow). (b) We induce Stark shifts to probe differential polarizabilities of ground ro-vibrational states with 1.95 μm light. (c) Example light shift measurement. The encircled data point corresponds to the spectrum shown in (b).

ence between the two Raman lasers. In addition to stabilizing our clock lasers, we rely on magic-wavelength trapping in order to reduce broadening of the linewidth. Our method for magic trapping utilizes polarizability crossings generated by the dispersive behavior of the target state polarizability near transitions to the electronically excited $(1)\, 1_u$ potential [9]. We select $(1)\, 1_u$ states such that the line strength S [42] is greater than $\sim 10^{-5}\,(ea_0)^2$ (here e is the electron charge, a_0 is the Bohr radius). Large line strengths correspond to large magic detunings, allowing for molecular lifetimes of a few ms, and corresponding Fourier-limited linewidths of 1 kHz or better. Our lattice wavelength is stabilized to a wavemeter at $\sim 100\,$MHz precision.

To determine differential polarizabilities, we induce ac Stark shifts on these clock transitions using an additional 1.95 μm laser. We typically observe ac Stark shifts of up to 20 kHz [as shown for $0 \leftrightarrow 62$ in Fig. 1(b)]. We measure ac Stark shifts of each transition as a function of 1.95 μm laser power [Fig. 1(c)] relative to the $27 \leftrightarrow 62$ transition. We do not observe any significant hyperpolarizability [41] effects in the ac Stark shift at 1.95 μm and therefore we fit a simple proportion. To determine the differential polarizability, we need to adequately characterize the intensity of the 1.95 μm probe light at our molecules. We calibrate the intensity of the 1.95 μm light by comparing the ac Stark shift of the $27 \leftrightarrow 62$ transition to that of the $\Delta m = 0$ component of atomic intercombination $^1S_0 \rightarrow ^3P_1$ transition with a differential polarizability of $+326.2(3.6)$ a.u. [50]. For our maximum power of 1.7 W of 1.95 μm power, we have an intensity of 8.551×10^5 W/cm^2. For most transitions, this scheme allows us to determine the differential polarizabilities to 5% as listed in Table I and shown in Fig. 2.

To determine the corresponding BBR shifts, we need a method to model the differential polarizabilities at all wave-
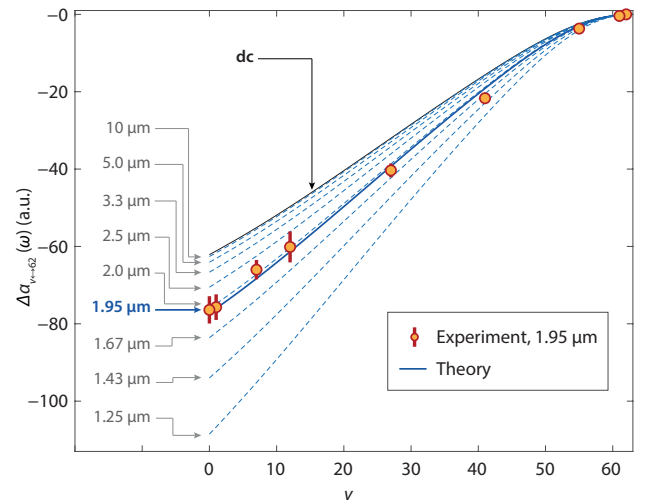
strengths, and requires several diode lasers in the 727–735 nm and 760–800 nm wavelength ranges.

We initially locate the target vibrational states v using Autler-Townes spectroscopy. While high-precision absolute determinations of these binding energies are beyond the scope of this Letter, we list the vibrational splittings $f_{v \leftrightarrow v'}$ to ~ 100 kHz precision (Table I). We estimate the uncertainty as fully dominated by lattice light shift [46].

We employ several strategies to achieve 1 kHz spectroscopic resolution, which enables us to determine ac Stark shifts to ~ 100 Hz using Lorentzian fits. After initially locating the transitions, we switch to a Raman configuration by detuning +30 MHz from the intermediate resonance in order to narrow down our transition linewidth. We stabilize the pump laser to a high finesse ($>3 \times 10^5$) cavity using a Pound-Drever-Hall lock [48, 49], which in turn serves as a stable reference for the repetition rate of an optical frequency comb. We then lock our anti-Stokes clock laser to the frequency comb. This locking scheme ensures the stability of the frequency differ-

FIG. 2. Differential polarizability with respect to the least-bound $v = 62$ state in ground state Sr_2. Points denote experimentally measured ac polarizabilities at $\lambda = 1.95$ μm. Lines are *ab initio* polarizabilities from dc to $\lambda = 1.25$ μm.

TABLE I. Bound states of the ^{88}Sr$_2$ molecule investigated in this work. The initial molecular state is always the rotationless near-threshold $v' = 62$ level. Here v denotes the vibrational quantum number of the target bound state in the electronic ^{1}S$_0$+^{1}S$_0$ 0_g^+ ground state and λ_{magic} is the magic wavelength. The differential polarizabilities are expressed in atomic units of $e^2 a_0^2/E_h$, where e is the electron charge, a_0 is the Bohr radius and E_h is the Hartree energy [47].

Clock transitions					Differential polarizability $\alpha_{v\leftrightarrow v'}(\omega)$ (a.u.)			
$X\,0_g^+\ v \leftrightarrow v'$	v''	$f_{v\leftrightarrow v'}$ (MHz)	$\tilde{R}_v$ (a.u.)	λ_{magic} (nm)	Experiment (1.95 µm)	Theory (1.95 µm)	Theory (dc)	$\Delta f_{v\leftrightarrow v'}$ (Hz)
$61 \leftrightarrow 62$	15	1263.673 58(20) [45]	43.6	–	−0.41(0.52)	−0.13	−0.11	+9.32(25) × 10^{-4}
$55 \leftrightarrow 62$	15	108 214.221(78)	21.6	–	−3.68(0.38)	−2.98	−2.43	+0.020 99(56)
$41 \leftrightarrow 62$	11	2 177 876.735(88)	13.6	996.4379	−21.67(0.88)	−19.1	−15.6	+0.134 9(37)
$27 \leftrightarrow 62$	11	8 075 406.28(10)	11.1	1006.5787	−40.4(1.8)	−39.3	−32.0	+0.276 8(75)
$12 \leftrightarrow 62$	16	19 176 451.65(11)	9.62	1007.7634	−60.1(4.0)	−61.3	−49.7	+0.430(12)
$7 \leftrightarrow 62$	15	24 031 492.42(12)	9.27	1007.1334	−66.0(2.5)	−68.3	−55.1	+0.477(13)
$1 \leftrightarrow 62$	11	30 640 159.75(12)	8.91	1016.9714	−75.7(3.3)	−76.0	−61.1	+0.529(15)
$0 \leftrightarrow 62$	11	31 825 183.207 5928(51) [41]	8.86	1004.7720	−76.4(3.6)	−77.2	−62.1	+0.538(15)

lengths from dc to infrared. The overwhelming majority of the BBR spectral energy density falls below 2 µm. While we cannot experimentally probe this entire range of wavelengths, we can leverage close agreement between theory and experiment at 1.95 µm and extend theoretical models to provide a full description of the BBR shift. We use modern quantum chemistry methods to calculate the differential polarizabilities for all molecular clock transitions in two steps: first, we calculate *ab initio* electronic polarizabilities of the strontium dimer as a function of internuclear distance R, and second, we ob-

tain the polarizability for each vibrational level as an average of the electronic polarizability over the vibrational wavefunction.

In homonuclear molecules, only electronic transitions contribute to polarizabilities and BBR shifts. To first calculate the electronic polarizability, we employ the approach based on asymmetric analytical derivative of the coupled-cluster energy with single and double excitations (CCSD) [53], as implemented in the Q-Chem 5 package [54]. We use the ECP28MDF pseudopotential together with its dedicated valence basis set [55]. For any given lattice light frequency ω, we first calculate the interaction-induced polarizability of Sr$_2$ molecules, $\alpha_{ij}^{\mathrm{int}}(\omega;R) = \alpha_{ij}(\omega;R) - 2\alpha_{\mathrm{atom}}(\omega)$, where $\alpha_{ij}(\omega)$ are tensor components of the total molecular polarizability and $\alpha_{\mathrm{atom}}(\omega)$ is the atomic polarizability at frequency ω. Since we are working only with isotropic $J = 0$ states, we take the trace polarizability $\alpha^{\mathrm{int}}(\omega;R) = [\alpha_{zz}^{\mathrm{int}}(\omega;R) + 2\alpha_{xx}^{\mathrm{int}}(\omega;R)]/3$ [56, 57]. We extend the model for large R using a fitted long-range form $\alpha^{\mathrm{int}}(\omega;R) \sim A_6(\omega)R^{-6} + A_8(\omega)R^{-8} + A_{10}(\omega)R^{-10}$ [58]. Figure 3 shows the isotropic component $\alpha^{\mathrm{int}}(\omega;R)$ at 1.95 µm as a function of R.

In the second step, we calculate the polarizability of each vibrational level v by averaging the electronic polarizability $\alpha^{\mathrm{int}}(R)$ over the level's vibrational wavefunction $\Psi_v(R)$:

$$\alpha_v^{\mathrm{int}}(\omega) = \int_0^\infty |\Psi_v(R)|^2\, \alpha^{\mathrm{int}}(\omega;R)dR \qquad (1)$$

where the differential polarizability for a transition $v \leftrightarrow v'$ is

$$\Delta\alpha_{v\leftrightarrow v'}(\omega) = \alpha_{v'}^{\mathrm{int}}(\omega) - \alpha_v^{\mathrm{int}}(\omega) \qquad (2)$$

We obtain the vibrational wavefunctions by solving the radial Schrödinger equation, $[-(\hbar^2/2\mu)(d^2/dR^2) + V(R)]\Psi_v(R) = E_v\Psi_v(R)$, using a matrix discrete variable representation (DVR) method [59, 60]. We use an accurate molecular potential $V(R)$ derived from Fourier-transform spectroscopy [61], and the reduced mass μ equals half the mass of a Sr atom. Figure 2 shows calculated differential dc and ac polarizabilities for $v \leftrightarrow 62$ transitions. It should be noted that this approach is
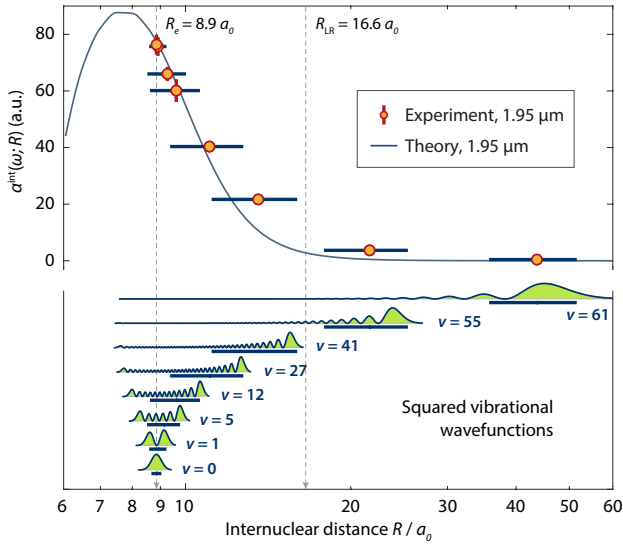

FIG. 3. Interaction-induced ac polarizability at $\lambda = 1.95$ µm. In addition to the *ab initio* result we show absolute experimental polarizabilities in relation to mean internuclear distances $\tilde{R}$ (Table I). Horizontal bars indicate the range $[\tilde{R}_v - S_{R_v},\ \tilde{R}_v + S_{R_v}]$ of internuclear distances probed by the vibrational wavefunctions shown in the lower panel. Here $\tilde{R}_v$ and S_{R_v} are the mean and standard deviation internuclear distances for wavefunction squared treated as a probability distribution. R_e and R_{LR} are, respectively, the equilibrium distance and the LeRoy radius [51, 52].

valid only when the adiabaticity condition is maintained, that is, that the ground-state potential does not cross any of the excited-state potentials if shifted upwards by the lattice photon energy. In Sr$_2$, the adiabaticity requirement limits the photon wavenumber to about 8000 cm^{-1} (1.25 μm). Both our ac Stark shift measurements 5128 cm^{-1} (1.95 μm) and the dominant spectral energy density of room temperature BBR are well within this margin.

We first validate the *ab initio* model using polarizabilities of the ground-state Sr atom. At dc we find a polarizability of +197.327 a.u., in excellent agreement with the state-of-the-art semi-empirical value of +197.14(20) a.u. [40]. Similarly, our ac polarizability of +207.524 a.u. at 1.95 μm agrees perfectly with the value of +208.2(1.1) a.u. [50].

The key test of our model relies on a direct comparison and strong agreement of measured molecular differential polarizability at 1.95 μm with the calculated values (Figure 2). For example, the theoretical differential polarizability for the $0 \leftrightarrow 62$ clock transition, $\Delta\alpha_{0\leftrightarrow62}(\omega)$, is -77.2 a.u. compared to the experimental value of $-76.4(3.6)$ a.u.. As we move to more weakly bound target states, the differential polarizabilities decrease monotonically. This can be elucidated using the R-centroid approximation [62] and the concept of a LeRoy radius R_{LR} [51, 52]. Firstly, the R-centroid approximation allows us to estimate the interaction-induced polarizability at the mean internuclear distance $\tilde{R}_v$ of state v using the differential polarizability of a $v \leftrightarrow 62$ transition:

$$\alpha^{\text{int}}(\omega; \tilde{R}_v) \approx -\Delta\alpha_{v\leftrightarrow62}(\omega), \quad (3)$$

where $\tilde{R}_v = \int_0^\infty |\Psi_v(R)|^2 R dR$. This formula neglects the small interaction-induced polarizability of the $v' = 62$ state. Thus, different vibrational transitions effectively serve as probes of polarizabilities, each at a different internuclear separation, as shown in Fig. 3.

The range of investigated target levels from the ground $v = 0$ state to the second-to-least bound $v = 61$ state spans internuclear distances from 8.86 a_0 (approximately the equilibrium distance R_e) to 43.6 a_0. Beyond the LeRoy radius of $R_{\text{LR}} = 16.6 \, a_0$ the interaction-induced polarizability is negligible: Sr$_2$ becomes a "physicist's molecule" [63] whose polarizability is squarely that of two strontium atoms. At shorter internuclear separations, it becomes a "chemist's molecule" and picks up over 80 a.u. of extra polarizability due to molecular bonding of the two consituent atoms. The qualitative boundary between the two extremes is set by $R_{LR} = 2(r_A + r_B)$, where $r_A = r_B = 4.15 \, a_0$ are the RMS charge radii of the two atoms [64]. By selecting vibrational levels with different mean internuclear distances, we scan the interaction-induced polarizabilities at different internuclear separations, interpolating between the two extremes of a "chemist's" and "physicist's" molecule.

To estimate the relative uncertainty of our theoretical model, we fit it to the experimental data by simple scaling. The best least-squares fit is achieved by scaling the model up by +1.8(2.4)%. This, however, is compatible with zero, implying that no model scaling is necessary; in fact, the reduced
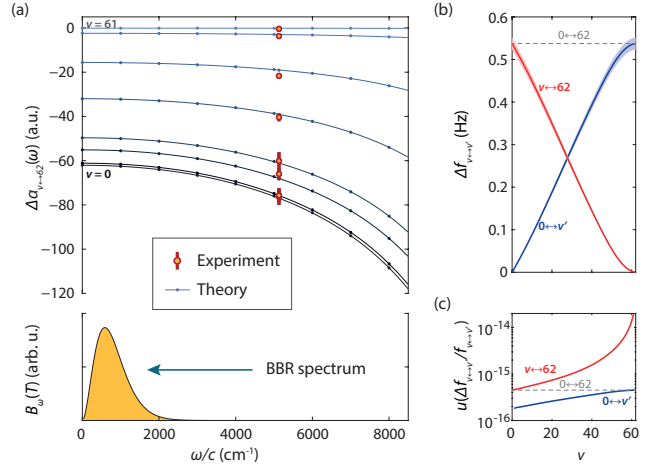

FIG. 4. (a) Differential polarizabilities for the selected clock transitions. Below, a plot of a BBR spectral energy density $u_\omega(T)$ at 300 K. (b) Absolute BBR shift for $0 \leftrightarrow v'$ clock transitions. (c) Relative BBR uncertainty for the same clock configurations.

chi-square $\chi^2/\text{dof} = 1.78$ for the scaled model (dof = 7) is worse than $\chi^2/\text{dof} = 1.69$ (dof = 8) for the original, unscaled model. Nevertheless, to estimate the accuracy of our theoretical model, we combine the 2.4% uncertainty from the scaling factor with an additional 1.8% possible systematic error to obtain a "Type B" uncertainty [65] of 2.6%.

Finally, we can proceed to calculating the BBR shifts. The BBR-induced shift $\Delta f_{v\leftrightarrow v'}$ can be expressed as an ac Stark shift integrated over the BBR spectrum [37, 39, 66]:

$$\Delta f_{v\leftrightarrow v'} = -\frac{1}{2h} \int_0^\infty \frac{4\pi}{\epsilon_0 c} B_\omega(T) \Delta\alpha_{v\leftrightarrow v'}(\omega) d\omega, \quad (4)$$

where the spectral radiance of the BBR field at temperature T is

$$B_\omega(T) = \frac{\hbar\omega^3}{4\pi^3 c^2} \frac{1}{\exp(\hbar\omega/k_B T) - 1}. \quad (5)$$

Typically, BBR shifts for atomic clocks are determined using a sum-over-states approach to calculate the static and dynamic terms [37, 38, 40, 66, 67], but here we already have computed the dynamic polarizabilities, so we can directly integrate the BBR shift. Since most of the BBR spectral energy density falls below any resonance frequencies in our system, we expand the polarizability in terms of Cauchy coefficients [67]: $\Delta\alpha_{v\leftrightarrow v'}(\omega) = \Delta\alpha_{v\leftrightarrow v'}^{(0)} + \Delta\alpha_{v\leftrightarrow v'}^{(2)}\omega^2 + \Delta\alpha_{v\leftrightarrow v'}^{(4)}\omega^4 + \ldots$ that we fit to tenth order to numerically calculated polarizabilities [Fig. 4(a)]. This allows us to express the BBR shift as a series:

$$\Delta f_{v\leftrightarrow v'} = \sum_{n=0,2,\ldots} \Delta f_v^{(n)} = \sum_{n=0,2,\ldots} -\frac{c_n \Delta\alpha_{v\leftrightarrow v'}^{(n)}}{4\pi^3 \epsilon_0 c^3} \left(\frac{k_B T}{\hbar}\right)^{4+n}, \quad (6)$$

where the Planck integrals $c_n = \int_0^\infty u^{3+n}/(e^u - 1) du$ are given in Table II. The leading term is the well known static contribution to the BBR shift [39, 40], while further terms constitute

TABLE II. Contributions to the BBR shift at 300 K for the $0 \leftrightarrow 1$ and $0 \leftrightarrow 62$ transitions.

n	c_n	$\Delta f_{0\leftrightarrow 1}^{(n)}$ (Hz)	$\Delta f_{0\leftrightarrow 1}^{(n)}/f_{0\leftrightarrow 1}$	$\Delta f_{0\leftrightarrow 62}^{(n)}$ (Hz)	$\Delta f_{0\leftrightarrow 62}^{(n)}/f_{0\leftrightarrow 62}$
0	$\pi^4/15$	+0.0081	$+6.8\times 10^{-15}$	+0.53	$+1.7\times 10^{-14}$
2	$8\pi^6/63$	$+6.1\times 10^{-5}$	$+5.1\times 10^{-17}$	+0.0033	$+1.0\times 10^{-16}$
4	$8\pi^8/15$	$+6.5\times 10^{-7}$	$+5.5\times 10^{-19}$	$+6.3\times 10^{-5}$	$+2.0\times 10^{-18}$
$\eta\,(\%)$		0.54		0.62	

a dynamic correction η on the order of 0.5–0.6 % (Table II). Here terms beyond the second order are negligible.

Since the molecular clock uniquely provides an array of available clock states, we calculate the BBR shift for other clock transitions. In Fig. 4(b), we plot the BBR shift for $v \leftrightarrow 62$ transitions, $\Delta f_{v\leftrightarrow 62}$ (red line). The BBR shift for our previously measured clock transition [41], $\Delta f_{0\leftrightarrow 62}$, is +538 mHz with a fractional uncertainty of 4.7×10^{-16}. We further find that the fractional uncertainty of the BBR shift can be reduced by strategically selecting $0 \leftrightarrow v'$ clock transitions (blue line) between deeply bound vibrational states [Fig. 4(c)]. This configuration could allow the fractional uncertainty to be as low as 1.8×10^{-16}, a factor of ~2.5 lower than the $0 \leftrightarrow 62$ transition.

In conclusion, we have precisely determined the BBR shift in a strontium molecular lattice clock. We do so by leveraging agreement between precision spectroscopy and modern quantum chemistry to provide a robust description of the polarizability behavior of ground state Sr_2 molecules. Specifically, we performed ac Stark shift spectroscopy of several molecular clock transitions throughout the ground state potential induced by an additional 1.95 μm laser. These measurements were in excellent agreement with *ab initio* calculations of molecular polarizability, lending credence to extending this model to other wavelengths from dc to 1.25 μm. This determination will allow us to control the BBR shift systematic to the 10^{-16} level. By selecting a clock transition between deeply bound vibrational states ($v < 10$), we could further suppress the BBR effect. In the future, additional measurements of ac or dc Stark shifts, such as by direct application of a dc electric field [37] or ac Stark measurement with a CO_2 laser [68, 69], could further constrain the theoretical model resulting in improved control of the BBR systematic. A next-generation molecular clock could search for new interactions beyond the Standard Model or probe the variations of fundamental constants. This work paves the way towards mHz-level spectroscopy in Sr_2 molecules.

* These authors contributed equally to this work.
† tanya.zelevinsky@columbia.edu

[1] M. Takamoto, F.-L. Hong, R. Higashi, and H. Katori, An optical lattice clock, Nature 435, 321 (2005).

[2] H. Katori, Optical lattice clocks and quantum metrology, Nature Photonics 5, 203 (2011).

[3] W. F. McGrew, X. Zhang, R. J. Fasano, S. A. Schäffer, K. Beloy, D. Nicolodi, R. C. Brown, N. Hinkley, G. Milani, M. Schioppo, T. H. Yoon, and A. D. Ludlow, Atomic clock performance enabling geodesy below the centimetre level, Nature 564, 87 (2018).

[4] T. Bothwell, D. Kedar, E. Oelker, J. M. Robinson, S. L. Bromley, W. L. Tew, J. Ye, and C. J. Kennedy, JILA SrI optical lattice clock with uncertainty of 2×10^{-18}, Metrologia 56, 065004 (2019).

[5] W. F. McGrew, X. Zhang, H. Leopardi, R. J. Fasano, D. Nicolodi, K. Beloy, J. Yao, J. A. Sherman, S. A. Schäffer, J. Savory, R. C. Brown, S. Römisch, C. W. Oates, T. E. Parker, T. M. Fortier, and A. D. Ludlow, Towards the optical second: verifying optical clocks at the SI limit, Optica 6, 448 (2019).

[6] J. Lodewyck, On a definition of the si second with a set of optical clock transitions, Metrologia 56, 055009 (2019).

[7] S. Bize, The unit of time: Present and future directions, Comptes Rendus Physique 20, 153 (2019).

[8] M. Borkowski, Optical Lattice Clocks with Weakly Bound Molecules, Physical Review Letters 120, 083202 (2018).

[9] S. S. Kondov, C.-H. Lee, K. H. Leung, C. Liedl, I. Majewska, R. Moszynski, and T. Zelevinsky, Molecular lattice clock with long vibrational coherence, Nature Physics 15, 1118 (2019).

[10] J. Kobayashi, A. Ogino, and S. Inouye, Measurement of the variation of electron-to-proton mass ratio using ultracold molecules produced from laser-cooled atoms, Nature Communications 10, 3771 (2019).

[11] D. Hanneke, B. Kuzhan, and A. Lunstad, Optical clocks based on molecular vibrations as probes of variation of the proton-to-electron mass ratio, Quantum Science and Technology 6, 014005 (2020).

[12] G. Barontini, L. Blackburn, V. Boyer, F. Butuc-Mayer, X. Calmet, J. R. Crespo López-Urrutia, E. A. Curtis, B. Darquié, J. Dunningham, N. J. Fitch, E. M. Forgan, K. Georgiou, P. Gill, R. M. Godun, J. Goldwin, *et al.*, Measuring the stability of fundamental constants with a network of clocks, EPJ Quantum Technology 9, 12 (2022).

[13] E. J. Salumbides, W. Ubachs, and V. I. Korobov, Bounds on fifth forces at the sub-Å length scale, Journal of Molecular Spectroscopy 300, 65 (2014).

[14] J. Biesheuvel, J.-P. Karr, L. Hilico, K. Eikema, W. Ubachs, and J. Koelemeij, Probing QED and fundamental constants through laser spectroscopy of vibrational transitions in HD+, Nature Communications 7, 10385 (2016).

[15] M. Borkowski, A. A. Buchachenko, R. Ciuryło, P. S. Julienne,

H. Yamada, Y. Kikuchi, Y. Takasu, and Y. Takahashi, Weakly bound molecules as sensors of new gravitylike forces, Scientific Reports **9**, 14807 (2019).

[16] B. Heacock, T. Fujiie, R. W. Haun, A. Henins, K. Hirota, T. Hosobata, M. G. Huber, M. Kitaguchi, D. A. Pushin, H. Shimizu, M. Takeda, R. Valdillez, Y. Yamagata, and A. R. Young, Pendellösung interferometry probes the neutron charge radius, lattice dynamics, and fifth forces, Science **373**, 1239 (2021).

[17] S. Schiller and V. Korobov, Tests of time independence of the electron and nuclear masses with ultracold molecules, Phys. Rev. A **71**, 032505 (2005).

[18] D. DeMille, S. Sainis, J. Sage, T. Bergeman, S. Kotochigova, and E. Tiesinga, Enhanced sensitivity to variation of me/mp in molecular pectra, Physical Review Letters **100**, 043202 (2008).

[19] K. Beloy, A. W. Hauser, A. Borschevsky, V. V. Flambaum, and P. Schwerdtfeger, Effect of Alpha variation on the vibrational spectrum of Sr_2, Phys. Rev. A **84**, 062114 (2011).

[20] S. Schiller, D. Bakalov, and V. I. Korobov, Simplest molecules as candidates for precise optical clocks, Phys. Rev. Lett. **113**, 023004 (2014).

[21] M. Kajita, G. Gopakumar, M. Abe, M. Hada, and M. Keller, Test of m_p/m_e changes using vibrational transitions in $n_2{}^+$, Phys. Rev. A **89**, 032509 (2014).

[22] M. Germann, X. Tong, and S. Willitsch, Observation of electric-dipole-forbidden infrared transitions in cold molecular ions, Nature Physics **10**, 820 (2014).

[23] P. Wcisło, P. Ablewski, K. Beloy, S. Bilicki, M. Bober, R. Brown, R. Fasano, R. Ciuryło, H. Hachisu, T. Ido, J. Lodewyck, A. Ludlow, W. McGrew, P. Morzyński, D. Nicolodi, M. Schioppa, M. Sekido, R. Le Targat, P. Wolf, X. Zhang, B. Zjawin, and M. Zawada, New bounds on dark matter coupling from a global network of optical atomic clocks, Science Advances **4**, eaau4869 (2018).

[24] M. S. Safronova, The search for variation of fundamental constants with clocks, Annalen der Physik **531**, 1800364 (2019).

[25] N. R. Hutzler, Polyatomic molecules as quantum sensors for fundamental physics, Quantum Science and Technology **5**, 044011 (2020).

[26] R. Lange, N. Huntemann, J. M. Rahm, C. Sanner, H. Shao, B. Lipphardt, C. Tamm, S. Weyers, and E. Peik, Improved limits for violations of local position invariance from atomic clock comparisons, Phys. Rev. Lett. **126**, 011102 (2021).

[27] R. Le Targat, L. Lorini, Y. Le Coq, M. Zawada, J. Guéna, M. Abgrall, M. Gurov, P. Rosenbusch, D. G. Rovera, B. Nagórny, R. Gartman, P. G. Westergaard, M. E. Tobar, M. Lours, G. Santarelli, A. Clairon, S. Bize, P. Laurent, P. Lemonde, and J. Lodewyck, Experimental realization of an optical second with strontium lattice clocks, Nature Communications **4**, 2109 (2013).

[28] S. Falke, N. Lemke, C. Grebing, B. Lipphardt, S. Weyers, V. Gerginov, N. Huntemann, C. Hagemann, A. Al-Masoudi, S. Häfner, S. Vogt, U. Sterr, and C. Lisdat, A strontium lattice clock with 3×10^{-17} inaccuracy and its frequency, New Journal of Physics **16**, 073023 (2014).

[29] T. Nicholson, S. Campbell, R. Hutson, G. Marti, B. Bloom, R. McNally, W. Zhang, M. Barrett, M. Safronova, G. Strouse, W. Tew, and J. Ye, Systematic evaluation of an atomic clock at 2×10^{-18} total uncertainty, Nature Communications **6**, 6896 (2015).

[30] S. B. Koller, J. Grotti, S. Vogt, A. Al-Masoudi, S. Dörscher, S. Häfner, U. Sterr, and C. Lisdat, Transportable optical lattice clock with 7×10^{-17} uncertainty, Phys. Rev. Lett. **118**, 073601 (2017).

[31] Y. Hisai, D. Akamatsu, T. Kobayashi, K. Hosaka, H. Inaba, F.-L. Hong, and M. Yasuda, Improved frequency ratio measurement with ^{87}Sr and ^{171}Yb optical lattice clocks at NMIJ, Metrologia **58**, 015008 (2021).

[32] N. Ohmae, M. Takamoto, Y. Takahashi, M. Kokubun, K. Araki, A. Hinton, I. Ushijima, T. Muramatsu, T. Furumiya, Y. Sakai, N. Moriya, N. Kamiya, K. Fujii, R. Muramatsu, T. Shiimado, and H. Katori, Transportable Strontium Optical Lattice Clocks Operated Outside Laboratory at the Level of 10^{-18} Uncertainty, Advanced Quantum Technologies **4**, 2100015 (2021).

[33] I. Ushijima, M. Takamoto, M. Das, T. Ohkubo, and H. Katori, Cryogenic optical lattice clocks, Nature Photonics **9**, 185 (2015).

[34] P. Ablewski, M. Bober, and M. Zawada, Emissivities of vacuum compatible materials: towards minimising blackbody radiation shift uncertainty in optical atomic clocks at room temperatures, Metrologia **57**, 035004 (2020).

[35] V. I. Yudin, A. V. Taichenachev, M. Y. Basalaev, O. N. Prudnikov, H. A. Fürst, T. E. Mehlstäubler, and S. N. Bagayev, Combined atomic clock with blackbody-radiation-shift-induced instability below 10^{-19} under natural environment conditions, New Journal of Physics **23**, 023032 (2021).

[36] T. Middelmann, C. Lisdat, S. Falke, J. S. R. Vellore Winfred, F. Riehle, and U. Sterr, Tackling the blackbody shift in a strontium optical lattice clock, IEEE Transactions on Instrumentation and Measurement **60**, 2550 (2011).

[37] T. Middelmann, S. Falke, C. Lisdat, and U. Sterr, High accuracy correction of blackbody radiation shift in an optical lattice clock, Phys. Rev. Lett. **109**, 263004 (2012).

[38] C. Lisdat, S. Dörscher, I. Nosske, and U. Sterr, Blackbody radiation shift in strontium lattice clocks revisited, Phys. Rev. Res. **3**, L042036 (2021).

[39] S. G. Porsev and A. Derevianko, Multipolar theory of blackbody radiation shift of atomic energy levels and its implications for optical lattice clocks, Phys. Rev. A **74**, 020502 (2006).

[40] M. S. Safronova, S. G. Porsev, U. I. Safronova, M. G. Kozlov, and C. W. Clark, Blackbody-radiation shift in the Sr optical atomic clock, Physical Review A **87**, 012509 (2013).

[41] K. H. Leung, B. Iritani, E. Tiberi, I. Majewska, M. Borkowski, R. Moszynski, and T. Zelevinsky, Terahertz vibrational molecular clock with systematic uncertainty at the 10^{-14} level, Phys. Rev. X **13**, 011047 (2023).

[42] K. H. Leung, I. Majewska, H. Bekker, C.-H. Lee, E. Tiberi, S. S. Kondov, R. Moszynski, and T. Zelevinsky, Transition strength measurements to guide magic wavelength selection in optically trapped molecules, Phys. Rev. Lett. **125**, 153001 (2020).

[43] K. H. Leung, E. Tiberi, B. Iritani, I. Majewska, R. Moszynski, and T. Zelevinsky, Ultracold $^{88}Sr_2$ molecules in the absolute ground state, New Journal of Physics **23**, 115002 (2021).

[44] T. Zelevinsky, M. M. Boyd, A. D. Ludlow, T. Ido, J. Ye, R. Ciuryło, P. Naidon, and P. S. Julienne, Narrow Line Photoassociation in an Optical Lattice, Physical Review Letters **96**, 203201 (2006).

[45] B. H. McGuyer, M. McDonald, G. Z. Iwata, M. G. Tarallo, A. T. Grier, F. Apfelbeck, and T. Zelevinsky, High-precision spectroscopy of ultracold molecules in an optical lattice, New J. Phys **17**, 055004 (2015).

[46] M. McDonald, B. H. McGuyer, G. Z. Iwata, and T. Zelevinsky, Thermometry via light shifts in optical lattices, Phys. Rev. Lett. **114**, 023001 (2015).

[47] E. Tiesinga, P. J. Mohr, D. B. Newell, and B. N. Taylor, Codata recommended values of the fundamental physical constants: 2018, Rev. Mod. Phys. **93**, 025010 (2021).

[48] R. V. Pound, Electronic frequency stabilization of microwave

oscillators, Review of Scientific Instruments **17**, 490 (1946).

[49] R. W. Drever, J. L. Hall, F. V. Kowalski, J. Hough, G. Ford, A. Munley, and H. Ward, Laser phase and frequency stabilization using an optical resonator, Applied Physics B **31**, 97 (1983).

[50] M. S. Safronova, private communication.

[51] R. J. Le Roy and R. B. Bernstein, Dissociation Energy and Long-Range Potential of Diatomic Molecules from Vibrational Spacings of Higher Levels, The Journal of Chemical Physics **52**, 3869 (1970).

[52] R. J. Le Roy, *Molecular Spectroscopy - Volume I, A Specialist Periodical Report of the Chemical Society* (The Chemical Society, London, 1973) pp. 113–171.

[53] K. D. Nanda and A. I. Krylov, Static polarizabilities for excited states within the spin-conserving and spin-flipping equation-of-motion coupled-cluster singles and doubles formalism: Theory, implementation, and benchmarks, The Journal of Chemical Physics **145**, 204116 (2016).

[54] E. Epifanovsky, A. T. B. Gilbert, X. Feng, J. Lee, Y. Mao, N. Mardirossian, P. Pokhilko, A. F. White, M. P. Coons, A. L. Dempwolff, Z. Gan, D. Hait, P. R. Horn, L. D. Jacobson, I. Kaliman, *et al.*, Software for the frontiers of quantum chemistry: An overview of developments in the Q-Chem 5 package, The Journal of Chemical Physics **155**, 084801 (2021).

[55] I. S. Lim, H. Stoll, and P. Schwerdtfeger, Relativistic small-core energy-consistent pseudopotentials for the alkaline-earth elements from Ca to Ra, The Journal of Chemical Physics **124**, 034107 (2006).

[56] A. Dalgarno, A. L. Ford, and J. C. Browne, Direct Sum-of-States Calculations of the Frequency-Dependent Polarizability of H_2, Physical Review Letters **27**, 1033 (1971).

[57] J. M. Brown and A. Carrington, *Rotational Spectroscopy of Diatomic Molecules* (Cambridge University Press, Cambridge, 2003).

[58] T. G. A. Heijmen, R. Moszynski, P. E. S. Wormer, and A. van der Avoird, Symmetry-adapted perturbation theory applied to interaction-induced properties of collisional complexes, Molecular Physics **89**, 81 (1996).

[59] D. T. Colbert and W. H. Miller, A novel discrete variable representation for quantum mechanical reactive scattering via the S-matrix Kohn method, J. Chem. Phys. **96**, 1982 (1992).

[60] E. Tiesinga, C. J. Williams, and P. S. Julienne, Photoassociative spectroscopy of highly excited vibrational levels of alkali-metal dimers: Green-function approach for eigenvalue solvers, Phys. Rev. A **57**, 4257 (1998).

[61] A. Stein, H. Knöckel, and E. Tiemann, $^1S+^1S$ asymptote of Sr_2 studied by Fourier-transform spectroscopy, Eur. Phys. J. D **57**, 171 (2010).

[62] P. A. Fraser, A method of determining the electronic transition moment for diatomic molecules, Canadian Journal of Physics **32**, 515 (1954).

[63] K. M. Jones, E. Tiesinga, P. D. Lett, and P. S. Julienne, Ultracold photoassociation spectroscopy: Long-range molecules and atomic scattering, Reviews of Modern Physics **78**, 483 (2006).

[64] E. Clementi, D. L. Raimondi, and W. P. Reinhardt, Atomic Screening Constants from SCF Functions. II. Atoms with 37 to 86 Electrons, J. Chem. Phys. **471**, 1300 (1967).

[65] B. N. Taylor and C. E. Kuyatt, *NIST Technical Note 1297. Guidelines for evaluating and expressing the uncertainty of NIST measurement results* (US Department of Commerce, Technology Administration, National Institute of Standards and Technology, 1994).

[66] J. W. Farley and W. H. Wing, Accurate calculation of dynamic stark shifts and depopulation rates of Rydberg energy levels induced by blackbody radiation. Hydrogen, helium, and alkali-metal atoms, Phys. Rev. A **23**, 2397 (1981).

[67] J. Mitroy, M. S. Safronova, and C. W. Clark, Theory and applications of atomic and ionic polarizabilities, Journal of Physics B: Atomic, Molecular and Optical Physics **43**, 202001 (2010).

[68] J. Chen, To simulate blackbody radiation frequency shift in cesium fountain frequency standard with CO_2 laser, IEEE Transactions on Ultrasonics, Ferroelectrics and Frequency Control **53**, 1685 (2006).

[69] K. J. Arnold, R. Kaewuam, A. Roy, T. R. Tan, and M. D. Barrett, Blackbody radiation shift assessment for a lutetium ion clock, Nature Communications **9**, 1650 (2018).